

Galaxy evolution in the cosmic web: the relative impact of nodes and filaments in the EAGLE simulation

Suman Sarkar ^a, Biswajit Pandey ^b, and Apashanka Das ^c

^aDepartment of Physics, Biswa Bangla Biswabidyalay, Bolpur, West Bengal - 731204, India.

^bDepartment of Physics, Visva-Bharati University, Santiniketan, West Bengal - 731235, India

^cHarish-Chandra Research Institute, HBNI, Chhatnag Road, Jhansi, Allahabad, 211109, India

E-mail: suman2reach@gmail.com, biswap@visva-bharati.ac.in,
a.das.cosmo@gmail.com

Abstract. Galaxies evolve within the intricate geometry of the cosmic web, yet the distinct physical roles of its primary components - nodes and filaments remain incompletely understood. Using the EAGLE cosmological hydrodynamical simulation, we investigate how proximity to filament spines and nodes jointly and independently regulates galaxy evolution. Galaxies are classified into red, green, and blue populations through a fully data-driven entropic thresholding method, while nodes and filaments are identified using the topological structure finder DisPerSE. We find that red galaxies preferentially inhabit regions close to both filament cores and nodes, whereas blue galaxies dominate the outskirts. This spatial segregation reveals two characteristic transition scales associated with filaments and nodes. The node-driven crossover occurs at ~ 2.5 Mpc, comparable to typical virial radii of group- and cluster-sized haloes, indicating that colour transformation becomes efficient once galaxies enter dynamically bound environments where tidal interactions, mergers, and gas stripping operate effectively. In contrast, the filament-driven crossover occurs at ~ 0.75 Mpc, tracing the transverse extent of dynamically influential filament cores, where transformation proceeds more gradually through the suppression or modulation of cold gas accretion. Adopting an information-theoretic framework, we show that the normalised mutual information between dominant mass component and colour increases with distance from nodes at fixed filament proximity. This demonstrates that cluster-scale environments partially erase the intrinsic mass-colour coupling, whereas filamentary environments preserve and enhance it. The effect is strongly mass dependent: low-mass galaxies exhibit pronounced environmental modulation, while high-mass systems show weaker sensitivity, reflecting the interplay between external tidal forces and internal binding energy. Our results establish cosmic web evolution as a scale-dependent process in which nodes act as nonlinear dynamical processors, while filaments function as extended regulators of anisotropic gas accretion.

Contents

1	Introduction	1
2	Data and Method of Analysis	3
2.1	The EAGLE simulations	3
2.2	Classifying red, blue, and green galaxies using entropic thresholding	4
2.3	Identifying the cosmic web environments using DisPerSE	6
2.4	Environmental trends in relative colour fractions and mass dependence	6
2.5	Normalised mutual information between mass content and colour	8
3	Results	9
3.1	Relative fractions of red, green, and blue galaxies in the d_f - d_n plane	10
3.2	Mass dependence of the relative fractions in the d_f - d_n plane	13
3.3	Environmental modulation of the mass-colour coupling using normalized mutual information (NMI)	15
3.4	Mass dependence of the NMI signal	16
4	Conclusions	17
5	Acknowledgements	19
6	Data availability	19

1 Introduction

Galaxies form and evolve within the cosmic web, a vast network of nodes, filaments, sheets, and voids that emerges from the gravitational amplification of primordial density fluctuations [1–11]. This large-scale structure provides the fundamental environment in which galaxies assemble their mass, acquire angular momentum, and regulate their star formation activity. While galaxy evolution is known to depend strongly on internal processes and host dark matter halo mass, it has become increasingly clear that the geometry of the cosmic web itself plays an independent and physically meaningful role, encoding information that cannot be fully captured by local overdensity alone.

Early observational studies already pointed to a close connection between galaxy populations and filamentary environments. Analyses of Sloan Digital Sky Survey (SDSS) data revealed correlations between galaxy luminosity, colour, morphology, and the degree of filamentarity of the galaxy distribution [12]. In particular, red galaxies and ellipticals were found to be more strongly associated with dense filament intersections, while blue spirals traced the extended filamentary network. Subsequent work showed that star-forming galaxies exhibit a more filamentary distribution than passive systems [13], highlighting the intertwined roles of intrinsic galaxy properties and large-scale environment. The explicit dependence of galaxy colour on cosmic web geometry has since been established with increasing clarity.

Direct evidence for active environmental processing within filaments has emerged from studies of galaxies infalling along supercluster-scale filaments. Investigations of filaments connecting rich clusters revealed enhanced star formation at intermediate distances from cluster

centres, followed by rapid suppression closer to nodes [14, 15]. These trends, particularly pronounced for dwarf galaxies, were attributed to galaxy-galaxy interactions and harassment in crowded infall regions, preceding gas stripping and quenching in dense cluster cores. Such results firmly established filaments as sites of significant “pre-processing”, rather than passive conduits of matter.

With the development of robust filament-identification techniques and the availability of large galaxy surveys, it has become possible to quantify galaxy properties as explicit functions of distance to filament spines. Studies using SDSS data demonstrated systematic gradients in morphology, colour, and star formation rate with proximity to filaments that persist even after controlling for local density and redshift [16]. Similar trends were observed at intermediate redshift using VIPERS, where massive and quiescent galaxies were found preferentially closer to filament axes, while low-mass star-forming galaxies occupied filament outskirts [17]. Crucially, these signals remain significant after removing the influence of nodes, reinforcing the notion that filament geometry encodes information beyond simple overdensity.

These observational findings are supported by analyses combining surveys and hydrodynamical simulations. Using COSMOS data and the HORIZON-AGN simulation, [18] detected transverse stellar mass and colour gradients around filaments that persist after accounting for nodes and local density. Similarly, [19] found strong mass and colour gradients with distance to filaments and nodes in both the GAMA survey and simulations, attributing these trends to anisotropic tidal fields and filament-driven assembly bias. Further evidence linking filamentary environments to gas depletion and quenching was provided by [20], who connected gradients in stellar mass, star formation rate, and quiescent fraction around filaments to the distribution of diffuse gas. Using SDSS data, [21] demonstrated that filaments host a higher fraction of red galaxies than sheets at fixed luminosity and local density, thereby isolating the effect of geometry from that of overdensity. Importantly, the bimodal nature of the galaxy colour distribution was found to persist across all environments, suggesting that transitions from the blue cloud to the red sequence can occur universally, but with efficiencies that depend on the surrounding large-scale structure.

Hydrodynamical simulations offer key physical insight into the mechanisms underlying these trends. Cold gas inflows along filaments can sustain star formation in specific mass regimes, while regions near nodes favour quenching through shock heating, enhanced merger activity, and gas stripping. Using the Simba simulation, [22] showed that star formation is significantly suppressed within $\lesssim 100$ kpc of filaments at low redshift, accompanied by reduced HI fractions and elevated metallicities. Comparisons across different simulation suites, including EAGLE and IllustrisTNG, reveal broad qualitative agreement on the existence of filament-driven effects, while highlighting model-dependent differences in the balance between gas accretion, heating, and feedback.

Galaxy colour provides a particularly powerful tracer of evolutionary state. The well-established bimodal colour distribution separates galaxies into the blue cloud and the red sequence [23–27], with the green valley representing a transitional population undergoing quenching [28, 29]. Blue galaxies typically sustain star formation through ongoing cold gas accretion, whereas red galaxies have largely exhausted or lost their gas reservoirs. Green valley systems exhibit intermediate properties, reflecting quenching pathways influenced by both internal feedback and environment [29–32]. Recent observational studies have shown that, at fixed stellar mass and local density, galaxies closer to filaments are redder and more gas poor [33, 34]. Complementary analyses based on tidal-tensor classifications further demonstrate that the scaling relations between galaxy properties depend sensitively on cosmic

web geometry [35–37]. A recent analysis [38] of SDSS DR18 data reveals a distinct bifurcation in galaxy evolution, where high mass galaxies are quenched in dense clusters but maintain star formation and disk-like morphologies in low-density sheets.

Despite this substantial progress, several key questions remain open. In particular, the combined influence of filaments and nodes on galaxy colour evolution and gas content has not yet been systematically quantified within a single, self-consistent framework. Moreover, many existing studies rely on fixed or subjective cuts in colour or star formation rate to define galaxy populations, potentially biasing conclusions regarding transitional systems such as the green valley. There is therefore a clear motivation for geometry-aware, data-driven approaches that explicitly account for both filamentary and nodal environments.

In this work, we address these issues using the EAGLE cosmological hydrodynamical simulation. Filaments and nodes are identified using the topological algorithm DisPerSE, which provides well-defined, scale-independent measures of distances to cosmic web features. Galaxies are classified into blue, green, and red populations using entropic thresholding, a recently proposed data-driven method that avoids subjective parameter choices [39]. Our primary goal is to investigate how stellar mass, gas mass, and host halo mass vary across the blue cloud, green valley, and red sequence as functions of distance to filament spines and nodes. By explicitly separating the roles of filaments and nodes, we aim to clarify how large-scale cosmic geometry regulates the balance between gas replenishment and depletion, thereby shaping galaxy colour evolution.

2 Data and Method of Analysis

2.1 The EAGLE simulations

This work is based on the EAGLE (Evolution and Assembly of GaLaxies and their Environments) project [40, 41], a suite of state-of-the-art cosmological hydrodynamical simulations designed to model galaxy formation within the standard Λ CDM framework. The simulations self-consistently follow the coupled evolution of dark matter and baryonic matter, incorporating key physical processes such as radiative cooling, star formation, stellar evolution, chemical enrichment, and feedback from stars and active galactic nuclei. A spatially flat cosmology is adopted, consistent with *Planck* results, with parameters $\Omega_\Lambda = 0.693$, $\Omega_m = 0.307$, $\Omega_b = 0.048$, and $H_0 = 67.77 \text{ km s}^{-1} \text{ Mpc}^{-1}$ [42]. The simulations evolve matter from an initial redshift of $z = 127$ to the present epoch ($z = 0$) within periodic, comoving cubic volumes of side lengths 25, 50, and 100 Mpc, using a modified version of the GADGET-2 code [43].

In this work, we analyse the largest EAGLE reference simulation, the 100 Mpc comoving box Ref-L0100N1504, at $z = 0$ (*snapnum* = 28). This volume provides an optimal balance between spatial resolution and statistical power, allowing for a robust characterisation of large-scale cosmic web structures while resolving galaxy-scale baryonic processes. The simulation contains $2 \times 1504^3 \approx 6.8$ billion particles, with initial particle masses of $1.81 \times 10^6 M_\odot$ for baryons and $9.70 \times 10^6 M_\odot$ for dark matter. At this resolution, galaxies with stellar masses above $\log(M_\star/M_\odot) \sim 8$ are well resolved, enabling reliable measurements of their stellar, gaseous, and photometric properties. Galaxies are identified using the standard EAGLE group-finding pipeline, in which dark matter haloes are first located using a friends-of-friends algorithm and substructures are subsequently identified with SUBFIND [44]. The positions of galaxies are defined by the minima of their gravitational potential, as provided in the Ref-L0100N1504_Subhalo catalogue [45]. To exclude non-physical or poorly resolved objects, we restrict the analysis to subhaloes satisfying the quality criterion *Spurious* = 0.

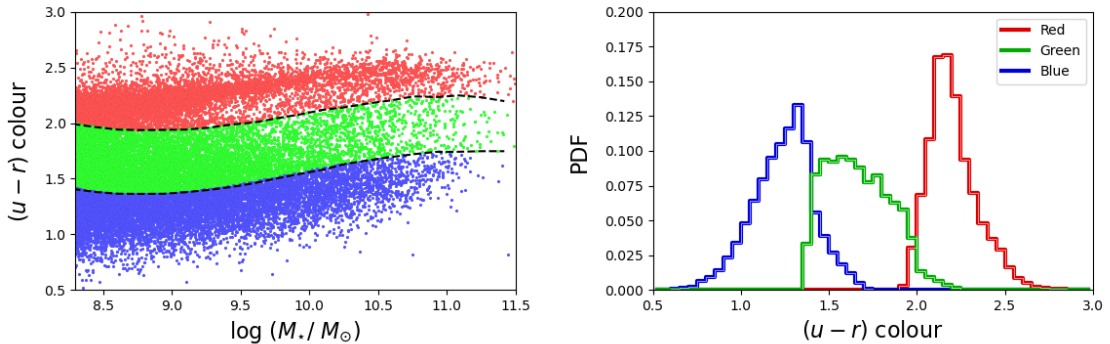


Figure 1. The left panel shows the red, green and blue galaxies identified using entropic thresholding on the $(u-r)$ colour-stellar mass plane. The PDFs of the three types of galaxy are shown in the right panel.

We extract a number of physical properties of the selected galaxies from the `Ref-L0100N1504_Aperture` catalogue, measured within a spherical aperture of comoving radius 30 kpc. These include stellar mass, gas mass, dark matter mass, and the rest-frame $(u-r)$ colour. The use of a fixed physical aperture ensures consistency across the galaxy population and facilitates direct comparisons between different evolutionary classes. We restrict our analysis to galaxies with stellar masses $\log(M_\star/M_\odot) \geq 8.3$, which corresponds to the lower mass limit above which reliable $(u-r)$ colour information is available in the EAGLE database. At this threshold, each galaxy is resolved by at least ~ 110 particles, ensuring robust measurements of both stellar and gaseous components. Applying these selection criteria yields a final sample of 29754 galaxies at $z=0$. This galaxy sample forms the basis for our analysis of how stellar mass, gas content, and halo properties vary across the blue cloud, green valley, and red sequence as functions of distance to filaments and nodes in the cosmic web.

2.2 Classifying red, blue, and green galaxies using entropic thresholding

Galaxy colour provides a direct observational proxy for evolutionary state, exhibiting a well-known bimodal distribution that separates star-forming systems in the blue cloud from passive galaxies in the red sequence, with the green valley occupying the intermediate, transitional regime. In this work, we adopt a fully data-driven approach to classify galaxies into blue, green, and red populations at $z=0$, using a combination of variance-based and entropy-based thresholding techniques.

As a first step, we identify the primary bimodality in the $(u-r)$ colour distribution using Otsu’s method, following [46]. This technique determines an optimal colour threshold that separates the full galaxy population into two classes by minimizing the variance within each class while simultaneously maximizing the variance between them. The two resulting populations correspond to the Blue Cloud (BC), dominated by star-forming galaxies with younger stellar populations, and the Red Sequence (RS), comprising predominantly passive galaxies with older stellar populations.

Formally, Otsu’s method minimizes the intra-class variance,

$$\sigma_{\text{intra}}^2 = P_{\text{BC}}\sigma_{\text{BC}}^2 + P_{\text{RS}}\sigma_{\text{RS}}^2, \quad (2.1)$$

while maximizing the inter-class variance,

$$\sigma_{\text{inter}}^2 = P_{\text{BC}}P_{\text{RS}}(\mu_{\text{BC}} - \mu_{\text{RS}})^2, \quad (2.2)$$

where P_{BC} and P_{RS} denote the probabilities of occurrence of the two classes, and μ and σ^2 represent their respective mean colours and variances. This procedure yields the characteristic mean colours μ_{BC} and μ_{RS} , which define the centres of the blue cloud and red sequence.

Otsu’s algorithm works by scanning through possible thresholds to find the one that best separates the classes. Essentially, it seeks a balance where the differences within each class are as small as possible, while the differences between classes are as large as possible. Interestingly, the threshold that achieves the lowest intra-class variance automatically produces the highest inter-class variance. This means that either σ_{intra}^2 or σ_{inter}^2 can be used interchangeably to identify the optimal threshold for red/blue classification.

While this binary classification robustly captures the dominant bimodality, it does not isolate the green valley population that lies between the two peaks. To explicitly identify this transitional class, we employ the entropic thresholding framework introduced by [39], which is based on the principle of maximum entropy [47]. This method enables an objective partitioning of the colour distribution into three statistically distinct classes without imposing arbitrary colour cuts.

The colour interval between μ_{BC} and μ_{RS} is first discretized into N bins, with $N = 30$ adopted in this work. Previous studies have shown that the resulting thresholds are not sensitive to the precise choice of bin number [39]. Two thresholds, s_1 and s_2 (with $s_1 < s_2$), are then identified within this interval by maximizing the total entropy,

$$H_{\text{total}} = H_{\text{BC}} + H_{\text{GV}} + H_{\text{RS}}, \quad (2.3)$$

where the entropy associated with each class is given by

$$H_{\text{BC}} = \log \left(\sum_{i=1}^{s_1} p_i \right) - \frac{\sum_{i=1}^{s_1} p_i \log p_i}{\sum_{i=1}^{s_1} p_i}, \quad (2.4)$$

$$H_{\text{GV}} = \log \left(\sum_{i=s_1+1}^{s_2} p_i \right) - \frac{\sum_{i=s_1+1}^{s_2} p_i \log p_i}{\sum_{i=s_1+1}^{s_2} p_i}, \quad (2.5)$$

$$H_{\text{RS}} = \log \left(\sum_{i=s_2+1}^N p_i \right) - \frac{\sum_{i=s_2+1}^N p_i \log p_i}{\sum_{i=s_2+1}^N p_i}, \quad (2.6)$$

with p_i denoting the probability associated with the i^{th} colour bin. The optimal values of s_1 and s_2 are obtained by iterating over all admissible threshold pairs and selecting the combination that maximizes H_{total} . This procedure partitions the galaxy population into three classes: the Blue Cloud ($(u-r) \leq s_1$), the Green Valley ($s_1 < (u-r) < s_2$), and the Red Sequence ($(u-r) \geq s_2$).

Since galaxy colour is known to correlate strongly with stellar mass, we perform this classification independently within discrete stellar mass bins. Within each mass bin, Otsu’s method is first applied to identify μ_{BC} and μ_{RS} , after which entropic thresholding is used to determine the green valley boundaries. This ensures that the colour cuts adapt dynamically with stellar mass, yielding a physically meaningful and internally consistent classification across the full mass range.

The left panel of Figure 1 illustrates the resulting thresholds in the colour–stellar mass plane, where the symbols indicate the entropic thresholds (s_1, s_2) in each mass bin and the solid curves show smooth cubic polynomial fits to these boundaries. The right panel of Figure 1 displays the resulting $(u-r)$ colour probability distribution functions for the blue,

green, and red galaxy populations at $z = 0$, demonstrating the effectiveness of the method in isolating the transitional green valley population.

2.3 Identifying the cosmic web environments using DisPerSE

In this work, we characterise the large-scale environment of galaxies in the EAGLE simulation by quantifying their geometric relationship to the cosmic web, specifically through their distances to filament spines and nodes. To this end, we identify filaments and nodes using the DIScrete PERsistent Structures Extractor (DisPerSE; [48, 49]), a scale-independent, topology-based algorithm designed to robustly map the filamentary structure of the cosmic web.

DisPerSE identifies cosmic web features by constructing the discrete Morse-Smale complex of the underlying density field. The density field is estimated from the discrete galaxy distribution using the Delaunay Tessellation Field Estimator (DTFE; [50, 51]), which provides an adaptive, resolution-independent reconstruction of the continuous density field. Based on this field, DisPerSE locates the critical points of the density gradient classified by their Morse index as minima, saddle points, and maxima and identifies the integral lines connecting them. In three dimensions, these critical points correspond to voids (index 0), walls (index 1), filaments (index 2), and nodes (index 3). Filament spines are traced by the Morse field lines connecting saddle points to maxima, while nodes correspond to the local maxima of the density field where multiple filaments intersect.

To ensure that only physically meaningful structures are retained and to suppress features arising from Poisson noise or sampling fluctuations, we apply a persistence threshold of 5σ , retaining only those topological features whose persistence exceeds this level. Persistence quantifies the robustness of a structure by measuring the contrast between paired critical points, thereby providing a natural, scale-independent criterion for distinguishing genuine cosmic web features from noise.

For each galaxy in the final sample, we compute two geometric quantities: the distance to the nearest filament spine, denoted as d_f , and the distance to the nearest node, denoted as d_n . These distances are evaluated in three-dimensional comoving space and provide complementary measures of a galaxy’s location within the cosmic web. Throughout this work, we use the pair (d_f, d_n) to characterise the cosmic web environment of galaxies, enabling us to disentangle the relative and combined influences of filamentary and nodal environments on galaxy properties.

2.4 Environmental trends in relative colour fractions and mass dependence

To understand how galaxies migrate between the blue cloud, green valley, and red sequence, it is essential to examine how these populations are distributed across the cosmic web. While individual galaxy properties inform specific evolutionary pathways, the relative fractions of red, green, and blue galaxies provide a direct statistical measure of environmental transformation efficiency.

Relative fractions are particularly informative because absolute number counts are strongly modulated by the underlying density field, which increases toward filament spines and nodes. In contrast, quantities such as red/total or blue/total isolate changes in population composition from simple variations in galaxy abundance. This enables a cleaner assessment of how the probability of belonging to a given colour class depends on cosmic web geometry.

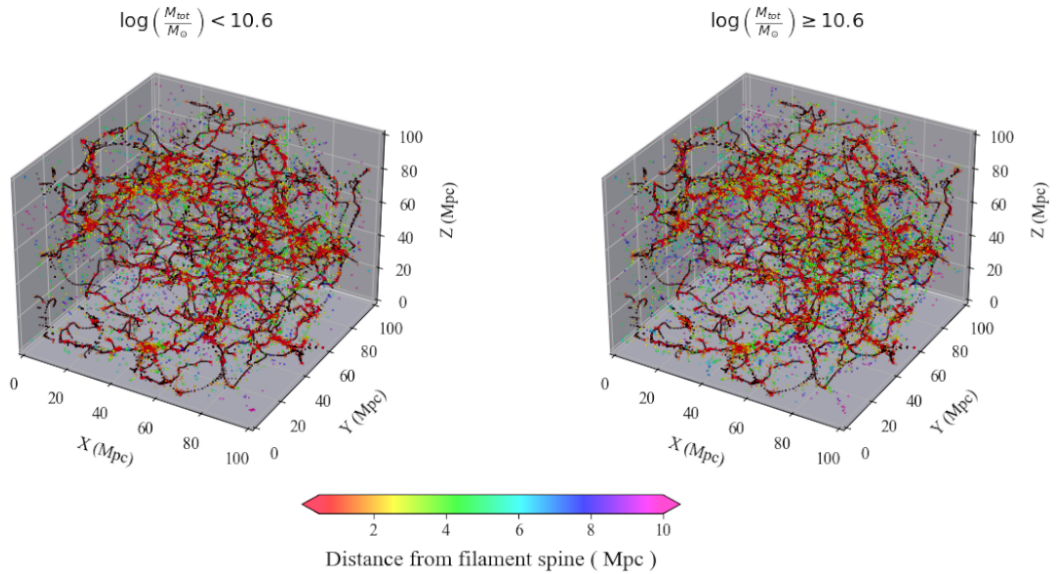


Figure 2. The two panels of this figure show filament spines and nodes identified with DisPerSE, overlaid with the spatial distribution of low-mass ($\log(M_{\text{tot}}/M_{\odot}) < 10.6$, left) and high-mass ($\log(M_{\text{tot}}/M_{\odot}) \geq 10.6$, right) galaxies. The colours indicate distance from the nearest filament spine.

Table 1. Classification of galaxies by dominant mass component using relative mass contrast Δ_m , with corresponding counts and percentages.

Galaxy class	Index	Criteria	Count (percentage)
Rich in stellar component	1	$\Delta_{\text{star}} \geq \Delta_{\text{gas}}$ & $\Delta_{\text{star}} > \Delta_{\text{DM}}$	5786 (24%)
Rich in dark matter	2	$\Delta_{\text{DM}} \geq \Delta_{\text{star}}$ & $\Delta_{\text{DM}} > \Delta_{\text{gas}}$	12576 (52%)
Rich in gas	3	$\Delta_{\text{gas}} \geq \Delta_{\text{DM}}$ & $\Delta_{\text{gas}} > \Delta_{\text{star}}$	6021 (25%)

We therefore study the variation of red, green, and blue fractions as functions of distance to the nearest node (d_n) and filament spine (d_f). These two measures trace physically distinct environments: nodes correspond to dynamically evolved, virialised regions dominated by mergers, tidal heating, and hot gas, whereas filaments represent anisotropic inflow channels where gas accretion and large-scale tides regulate galaxy growth more gradually. Examining colour fractions as independent functions of d_n and d_f allows us to disentangle their relative and combined influence.

This approach is closely related to anisotropic assembly bias, in which halo growth and baryonic accretion histories depend on large-scale tidal geometry at fixed mass. To assess how such environmental effects depend on intrinsic scale, we divide the sample at the median total mass, $\log(M_{\text{total}}/M_{\odot}) = 10.6$, producing statistically comparable low- and high-mass subsamples. This enables us to test whether colour transformations are primarily driven by mass, environment, or their coupled interplay across the cosmic web. We show the distribution of the low- and high- mass galaxies around the filament spines in the two panels of [Figure 2](#).

2.5 Normalised mutual information between mass content and colour

Galaxy colour encodes evolutionary state, while the relative contributions of dark matter, stars, and gas reflect the physical processes governing galaxy assembly. A natural question therefore arises: how strongly is the dominant mass component of a galaxy linked to its colour class?

One might attempt to address this by computing standard correlation coefficients between colour and individual mass components. However, such an approach is fundamentally limited for three reasons. First, galaxy colour in our analysis is a discrete, non-ordinal variable (red, green, blue), whereas the mass components are continuous quantities with highly non-Gaussian distributions. Second, correlations such as Pearson’s r capture only linear dependencies and may fail to detect nonlinear or non-monotonic relationships. Third, the interplay between stellar, gas, and dark matter components is intrinsically multivariate and competitive where the dominance of one component necessarily suppresses the relative contribution of the others.

To capture the full statistical dependence between colour class and mass dominance without assuming linearity or specific functional forms, we employ the framework of information theory. In particular, we quantify the association using the normalised mutual information (NMI), which measures the total shared information between two discrete random variables, irrespective of the nature of their dependence [52]. This approach allows us to assess whether knowledge of a galaxy’s dominant mass component reduces uncertainty about its colour class, and vice versa.

For each galaxy, the stellar mass (M_{star}), gas mass (M_{gas}), and dark matter mass (M_{DM}) are known. We define the mass fraction of a component m as

$$f_m = \frac{M_m}{M_{\text{tot}}}, \quad m \in \{\text{star, gas, DM}\}, \quad (2.7)$$

where

$$M_{\text{tot}} = M_{\text{star}} + M_{\text{gas}} + M_{\text{DM}}. \quad (2.8)$$

To characterise the relative dominance of each component, we introduce the mass contrast

$$\Delta_m = \frac{f_m}{\langle f_m \rangle} - 1, \quad (2.9)$$

where $\langle f_m \rangle$ is the sample-averaged mass fraction of component m . Each galaxy is then assigned a discrete mass-component index according to the dominant Δ_m , following the criteria summarised in Table 1. This procedure partitions the galaxy population into three physically interpretable classes: stellar-dominated, dark-matter-dominated, and gas-dominated systems.

Independently, galaxies are classified into red, green, and blue populations using the entropic thresholding technique described in subsection 2.2. Consequently, each galaxy is characterised by two categorical labels: one describing its dominant mass component and the other describing its colour class.

Consider a sample of N galaxies. Let n_j denote the number of galaxies in the j^{th} mass-component class and n_k the number in the k^{th} colour class, such that

$$\sum_{j=1}^3 n_j = \sum_{k=1}^3 n_k = N. \quad (2.10)$$

Let n_{jk} be the number of galaxies simultaneously belonging to mass-component class j and colour class k . These counts satisfy

$$\sum_k n_{jk} = n_j, \quad \sum_j n_{jk} = n_k, \quad \sum_j \sum_k n_{jk} = N. \quad (2.11)$$

The corresponding probabilities are

$$p(m_j) = \frac{n_j}{N}, \quad p(c_k) = \frac{n_k}{N}, \quad p(m_j, c_k) = \frac{n_{jk}}{N}. \quad (2.12)$$

The Shannon entropies associated with the mass-component classification, colour classification, and their joint distribution are defined as

$$H(M) = - \sum_{j=1}^3 p(m_j) \log p(m_j), \quad (2.13)$$

$$H(C) = - \sum_{k=1}^3 p(c_k) \log p(c_k), \quad (2.14)$$

$$H(M, C) = - \sum_{j=1}^3 \sum_{k=1}^3 p(m_j, c_k) \log p(m_j, c_k). \quad (2.15)$$

The mutual information between mass component and colour is

$$I(M; C) = H(M) + H(C) - H(M, C), \quad (2.16)$$

which quantifies the reduction in uncertainty in one variable given knowledge of the other. To facilitate comparison and interpretability, we normalise this quantity by the maximum possible entropy for three equally populated classes,

$$H_{\max} = \log 3, \quad (2.17)$$

and define the normalised mutual information as

$$I_{\text{N}}(M; C) = \frac{I(M; C)}{H_{\max}}. \quad (2.18)$$

By construction, $0 \leq I_{\text{N}} \leq 1$, where $I_{\text{N}} = 0$ indicates statistical independence between dominant mass component and colour class, and $I_{\text{N}} = 1$ indicates perfect association.

This information-theoretic measure provides a model-independent and non-parametric quantification of the coupling between galaxy mass composition and evolutionary state. Unlike linear correlation analyses, it captures the full structure of statistical dependence, including nonlinear, asymmetric, and multivariate effects. It therefore offers a more physically meaningful assessment of whether variations in dark matter, stellar, or gas dominance are genuinely linked to the transition between blue, green, and red galaxy populations.

3 Results

We now present the main findings of this work, focusing on how galaxy populations vary across the cosmic web and how the coupling between mass composition and colour depends on environment. We first examine the relative fractions of red, green, and blue galaxies as functions of distance from filament spines and nodes, and then quantify the environmental modulation of the mass-colour connection using an information-theoretic framework.

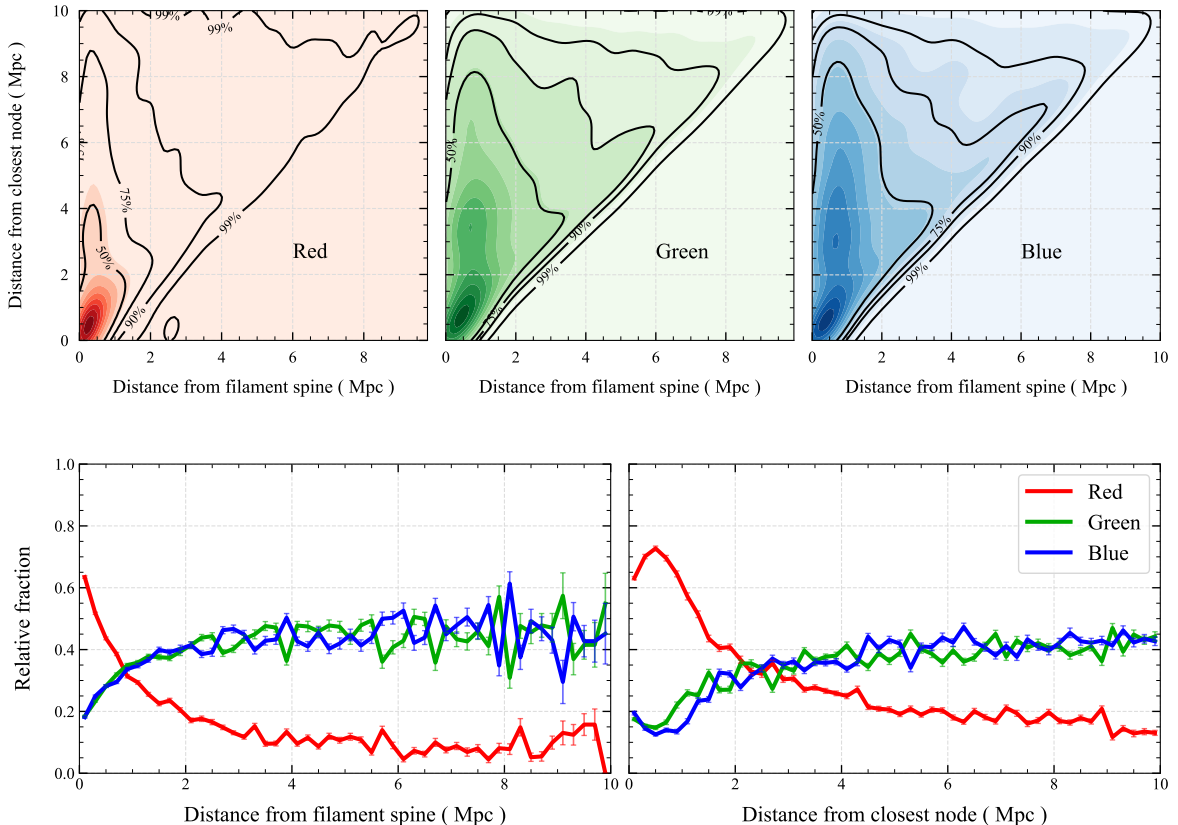


Figure 3. Top panels of this figure show joint probability distribution functions (PDF) of red (left), green (middle), and blue (right) galaxies in the d_f - d_n plane, where d_f and d_n denote distances from the filament spine and closest node, respectively. Contours enclose 50%, 75%, 90%, and 99% of each population. The bottom two panels show corresponding relative fractions as functions of d_f (left) and d_n (right). Red galaxies dominate near filament spines and nodes, while blue galaxies preferentially occupy larger distances. The crossover between red and blue fractions occurs at $d_f \sim 0.75$ Mpc and $d_n \sim 2.5$ Mpc for filament and node respectively. The 1σ error bars in each case are estimated using 100 jackknife samples drawn from the original distributions.

3.1 Relative fractions of red, green, and blue galaxies in the d_f - d_n plane

Figure 3 presents the environmental distribution of galaxy colour classes in the two-dimensional space defined by the distance to the filament spine (d_f) and the distance to the nearest node (d_n). The top panels show the joint probability density distributions of red-sequence, green-valley, and blue-cloud galaxies in the d_f - d_n plane, while the bottom panels display the corresponding relative fractions as one-dimensional functions of d_f and d_n .

The joint distributions reveal a clear geometric segregation of galaxy populations across the cosmic web. Red galaxies are strongly concentrated toward the lower-left region of the d_f - d_n plane, i.e., close to both filament spines and nodes. Their probability density peaks sharply at small d_f and small d_n , indicating that the densest and most dynamically evolved regions of the web preferentially host passive systems. In contrast, blue galaxies occupy a larger region of the parameter space. This behaviour is consistent with blue galaxies residing in relatively low-density, dynamically quiescent environments where gas accretion remains

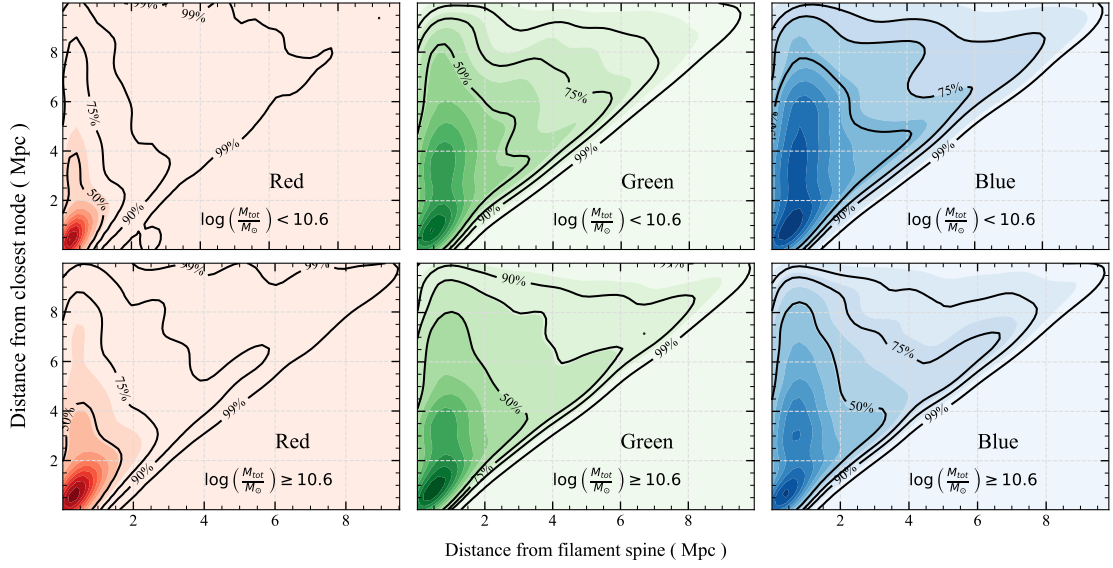


Figure 4. Joint PDF of red, green, and blue galaxies in the d_f - d_n plane, shown separately for $\log(M_{\text{tot}}/M_{\odot}) < 10.6$ (top) and $\log(M_{\text{tot}}/M_{\odot}) \geq 10.6$ (bottom). Low-mass galaxies exhibit stronger colour segregation with respect to filament and node proximity, whereas high-mass galaxies display a broader and less contrasted distribution.

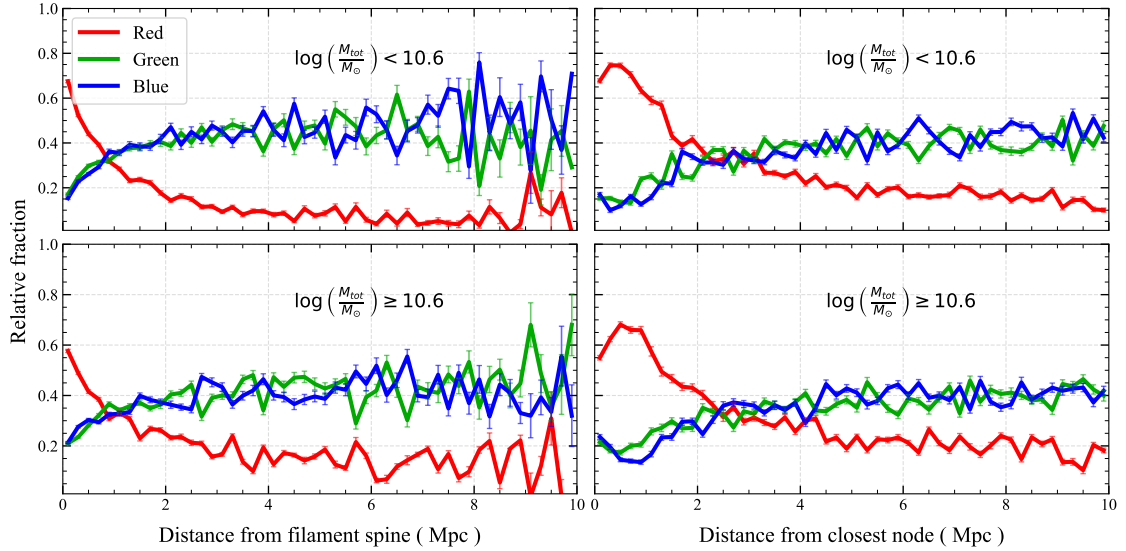


Figure 5. Relative fractions of red, green, and blue galaxies as functions of distance from the filament spine (left) and closest node (right), shown separately for $\log(M_{\text{tot}}/M_{\odot}) < 10.6$ (top) and $\log(M_{\text{tot}}/M_{\odot}) \geq 10.6$ (bottom). The 1σ errorbars are computed based on 100 jackknife resamplings of the underlying distributions.

efficient. Green-valley galaxies trace an intermediate distribution in the d_f - d_n plane. Their probability contours bridge the regions populated by red and blue systems, extending from filament interiors toward moderate node distances. This spatial continuity supports the interpretation of green-valley galaxies as a transitional population whose transformation is linked to gradual environmental modulation rather than abrupt dynamical events alone.

The bottom left panel of [Figure 3](#) shows the relative fractions of red, green, and blue galaxies as functions of d_f . A strong and monotonic environmental trend is evident. The red fraction decreases sharply with increasing distance from the filament spine, dropping from ~ 0.6 at $d_f \lesssim 1$ Mpc to $\lesssim 0.1$ beyond $d_f \sim 6$ – 8 Mpc. Conversely, the blue fraction rises steadily with increasing d_f , eventually dominating the population at $\gtrsim 0.75$ Mpc. Similarly, the green fraction peaks at intermediate distances and remains comparatively stable over a broad range of d_f . This behaviour demonstrates that proximity to filament spines is strongly associated with quenching. The monotonic decline of the red fraction with d_f suggests that filamentary environments regulate galaxy evolution in a systematic manner, likely through modulation of gas accretion and enhanced merger probabilities within the dynamically influential filament core.

The bottom right panel of [Figure 3](#) shows the variation of relative fractions with d_n . The red fraction is highest at small node distances, reaching ~ 0.7 at $d_n \lesssim 1$ Mpc, and decreases progressively with increasing d_n . In contrast, the blue fraction increases steadily with node distance. The crossover between red and blue populations occurs at $d_n \sim 2$ – 3 Mpc, marking a characteristic transition scale between node-dominated and filament-dominated regimes. Compared to the filament trends, the node dependence appears steeper at small d_n , consistent with rapid environmental processing within virialised regions. Nodes correspond to the densest and most dynamically evolved regions of the cosmic web, typically associated with massive haloes and clusters. As galaxies approach these environments, several quenching mechanisms become increasingly effective: ram-pressure stripping, tidal interactions, harassment, and shock heating of infalling gas. These processes efficiently remove or heat the cold gas reservoirs of galaxies, thereby suppressing star formation and increasing the red fraction. This naturally explains the monotonic rise in the red fraction with decreasing d_n . Interestingly, we observe a turnover in the red fraction at $d_f \lesssim 0.5$ Mpc. The turnover in the red fraction at smaller d_n likely reflects the competing interplay between environmental quenching and dynamical selection effects in the innermost cluster regions. Galaxies are particularly vulnerable to tidal disruption and merging in high-density cores. Consequently, the very central regions may become increasingly dominated by massive galaxies and remnants of previous mergers, reducing the number of surviving red systems. In addition, recently accreted galaxies undergoing rapid environmental transformation may temporarily populate intermediate colour states, thereby lowering the instantaneous red fraction in the very central regions.

Altogether, [Figure 3](#) reveals a coherent and physically interpretable pattern. The red galaxies preferentially inhabit regions close to both filament spines and nodes whereas the blue and green galaxies dominate in the outskirts of the web. The monotonic trends with d_f and d_n indicate that both components of the cosmic web contribute to galaxy transformation, albeit potentially through distinct mechanisms.

These results establish a baseline environmental dependence for the full galaxy sample. In the following subsections, we examine whether these trends persist or change when the population is separated into low- and high-mass subsamples, thereby probing the interplay between intrinsic mass scale and cosmic web geometry in driving galaxy evolution.

3.2 Mass dependence of the relative fractions in the d_f - d_n plane

To disentangle the interplay between intrinsic mass scale and large-scale environment, we also examine the same statistics separately for low-mass ($\log(M_{\text{tot}}/M_{\odot}) < 10.6$) and high-mass ($\log(M_{\text{tot}}/M_{\odot}) \geq 10.6$) galaxies. [Figure 4](#) and [Figure 5](#) present the corresponding two-dimensional distributions and relative fractions for these subsamples.

The two-dimensional d_f - d_n distributions in [Figure 4](#) reveal that the geometric segregation identified in [Figure 3](#) persists in both mass regimes, but with notable differences in strength. For low-mass galaxies, the red population remains relatively more concentrated toward small d_f and small d_n , while the existence of blue galaxies extend to larger distances from both structures. The contrast between red- and blue-dominated regions is particularly sharp, indicating that low-mass systems respond strongly to cosmic web geometry. For high-mass galaxies, the segregation is somewhat weaker. Red systems are more broadly distributed across the d_f - d_n plane, and blue galaxies are less spread out across the outskirts. This broader spread suggests that colour in massive galaxies is less exclusively controlled by their location in the cosmic web and more influenced by internal processes.

These differences become clearer in the one-dimensional trends observed in [Figure 5](#). For low-mass galaxies, the red fraction declines steeply with increasing distance from both filament spines and nodes. Near nodes ($d_n \lesssim 1$ Mpc), red galaxies dominate, while blue galaxies rapidly take over beyond $d_n \sim 2.5$ Mpc. Similarly, the red fraction decreases monotonically with increasing d_f , and the crossover between red and blue populations occurs at comparable filament distances as in the full sample. The environmental modulation is therefore strong and systematic in this mass regime. For high mass population, the red galaxies are still more common near nodes and filament spines. However the red fraction becomes less pronounced overall. This indicates that, for massive systems, colour transformation is less tightly coupled to cosmic web position.

It may be noted that in contrast to nodes, the red fraction increases monotonically with decreasing distance to filament spines for all mass ranges considered. No turnover is observed at small d_n , and the crossover between red and blue populations consistently occurs at ~ 0.75 Mpc, independent of total mass. This behaviour suggests that filaments act as sites of gradual, large-scale environmental modulation rather than abrupt dynamical transformation. Galaxies closer to filament spines reside in regions of enhanced matter inflow, anisotropic tidal forces, and elevated merger probabilities. The steady increase in red fraction toward filament centres is consistent with a scenario of “cosmic web starvation”, where gas accretion is progressively reduced or heated due to filamentary shocks and interactions, leading to a gradual suppression of star formation. Unlike nodes, filaments lack extremely dense cores where tidal destruction or rapid merging would significantly alter the surviving population statistics. Consequently, the red fraction does not exhibit a central turnover.

Taken together, [Figure 4](#) and [Figure 5](#) demonstrate that environmental colour segregation is strongly mass dependent. Low-mass galaxies exhibit pronounced gradients with both d_f and d_n , consistent with their greater susceptibility to external processes such as gas stripping, tidal heating, and suppression of accretion. High-mass galaxies, possessing deeper gravitational potentials and more efficient internal feedback, show weaker environmental gradients, implying that internal quenching mechanisms compete with or dominate over large-scale environmental effects.

These results suggest that cosmic web quenching operates most efficiently in low-mass systems, where environmental modulation can significantly alter the population mix across megaparsec scales. For massive galaxies, the imprint of large-scale geometry remains visible

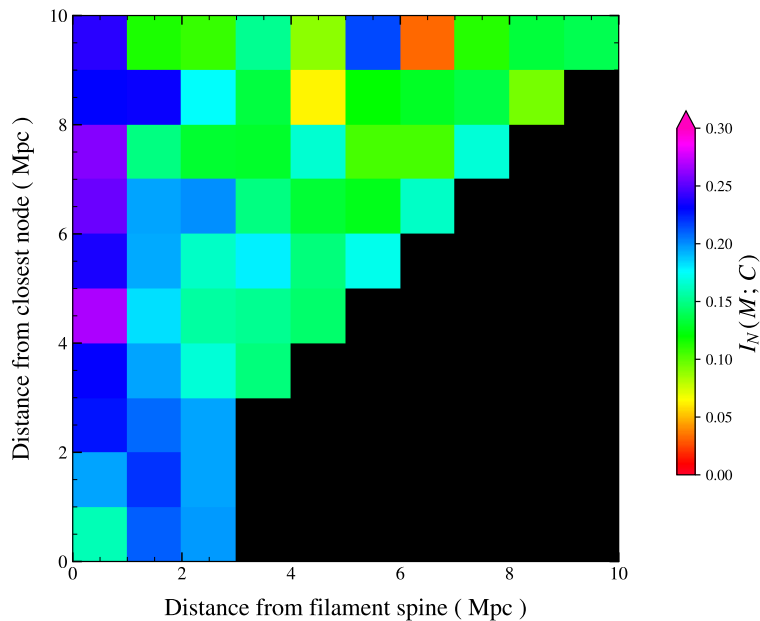


Figure 6. This shows the Normalised mutual information $I_N(M; C)$ between dominant mass component and galaxy colour across the d_f - d_n plane. Higher values indicate stronger statistical coupling. The black region corresponds to geometrically inaccessible combinations of (d_f, d_n) where no galaxies are present. The coupling strengthens in filament-dominated regions far from nodes and weakens near nodes.

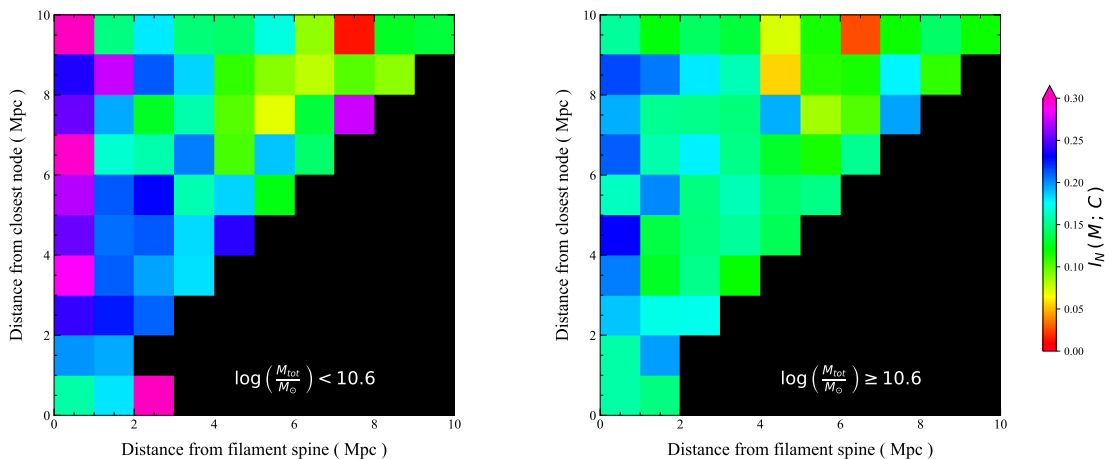


Figure 7. This shows the Normalised mutual information $I_N(M; C)$ in the d_f - d_n plane for low-mass galaxies ($\log(M_{\text{tot}}/M_{\odot}) < 10.6$, left) and high-mass galaxies ($\log(M_{\text{tot}}/M_{\odot}) \geq 10.6$, right). The environmental modulation is stronger for low-mass systems, while high-mass galaxies exhibit a flatter dependence on cosmic web geometry.

but is partially diluted by mass-driven evolutionary pathways. The combined analysis of Figure 3-Figure 5 therefore reveals a coherent picture in which the impact of filaments and nodes on galaxy colour is both scale dependent and intrinsically linked to galaxy mass.

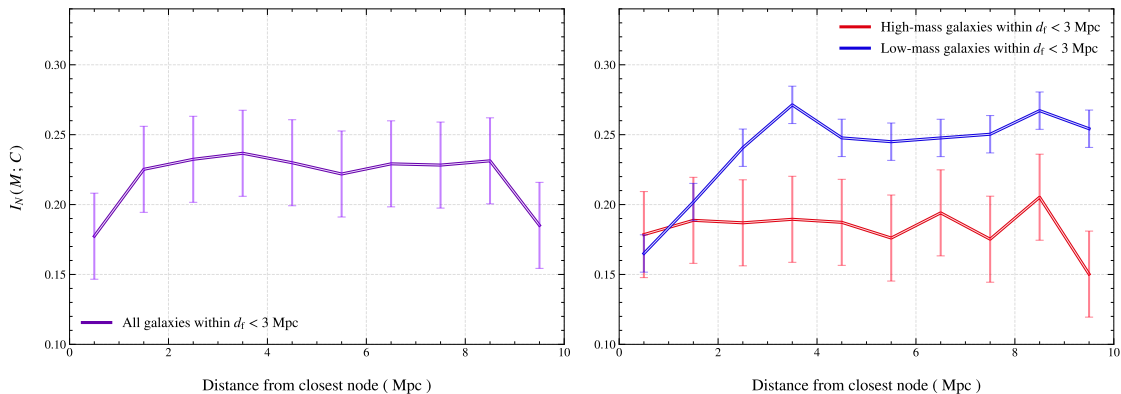


Figure 8. Normalised mutual information $I_N(M; C)$ as a function of node distance d_n for galaxies within $d_f < 3$ Mpc. Left panel show the result for full galaxy sample and right panel shows the comparison between low-mass ($\log(M_{\text{tot}}/M_\odot) < 10.6$) and high-mass ($\log(M_{\text{tot}}/M_\odot) \geq 10.6$) galaxies. Error bars represent 1σ uncertainties estimated from 100 jackknife resamplings. The increasing trend of I_N with d_n highlights the weakening of the mass-colour coupling in the vicinity of nodes particularly for low-mass systems.

3.3 Environmental modulation of the mass-colour coupling using normalized mutual information (NMI)

We now quantify how the statistical coupling between dominant mass component and galaxy colour varies across the cosmic web using the normalised mutual information $I_N(M; C)$. [Figure 6](#) shows the spatial distribution of I_N across the d_f - d_n plane for the full galaxy sample. A clear and systematic environmental trend is evident. At small filament distances ($d_f \lesssim 2$ Mpc), I_N increases steadily with increasing node distance. For example, at a fixed $d_f = 1$ Mpc, the normalised mutual information rises from $I_N \approx 0.15$ at $d_n \sim 1$ Mpc to $I_N \approx 0.28$ at $d_n \sim 8$ Mpc. This nearly twofold increase indicates that the predictive power of a galaxy’s dominant mass component for determining its colour strengthens significantly as one moves away from nodes while remaining embedded within the filament environment.

Near nodes, galaxies experience intense dynamical processing such as tidal interactions, ram-pressure stripping, and enhanced merger activity which can drive colour transformation independently of the galaxy’s initial baryonic configuration. Such externally driven quenching partially erases the intrinsic link between mass composition and star formation activity, thereby lowering I_N . At larger node distances, where cluster-scale tidal fields weaken and filamentary regulation dominates, galaxy evolution proceeds more gradually through modulation of gas accretion. In this regime, gas-rich systems preferentially remain blue while gas-poor or stellar-dominated systems migrate toward the red sequence, restoring a tighter correspondence between internal structure and colour.

The I_N map further reveals that the highest values ($I_N \gtrsim 0.25$) occur in regions that are close to filaments but far from nodes. This pattern reinforces the interpretation that filament-driven quenching is structurally mediated and mass-dependent, whereas node-driven quenching introduces an additional dynamical channel that partially decouples colour from mass composition. At large d_f , where both filamentary influence and gas regulation weaken, I_N decreases again, suggesting that the structural imprint of baryonic composition on colour is strongest within the dynamically influential filament core.

3.4 Mass dependence of the NMI signal

Figure 7 shows the corresponding I_N distributions after dividing the sample at the median total mass. The left panel presents low-mass galaxies ($\log(M_{\text{tot}}/M_{\odot}) < 10.6$), while the right panel shows high-mass systems ($\log(M_{\text{tot}}/M_{\odot}) \geq 10.6$).

For low-mass galaxies, the environmental trend seen in the full sample is reproduced with comparable or even enhanced contrast. At fixed filament distance, I_N increases strongly with node distance, reaching values $I_N \gtrsim 0.28$ in regions that are filament-dominated but node-remote. This confirms that low-mass systems are particularly sensitive to the competing influences of nodal processing and filamentary gas regulation. Their shallower potential wells render them more vulnerable to tidal stripping and ram-pressure effects near nodes, which efficiently disrupt the intrinsic mass-colour coupling and suppress I_N .

In contrast, for high-mass galaxies the I_N map is noticeably flatter. Although modest environmental variation persists, the amplitude of change with node distance is significantly reduced. Even near nodes, I_N does not decline as sharply as in the low-mass case. This suggests that massive galaxies retain a comparatively stable relationship between mass composition and colour across environments. Their deeper gravitational potentials and more efficient internal feedback processes reduce susceptibility to environmental decoupling, so that external dynamical processing near nodes does not substantially erase the structural imprint of baryonic composition.

Figure 8 reveals a distinct environmental modulation of the mass-colour coupling. In the full sample (left panel), the normalised mutual information I_N increases steadily with node distance up to $d_n \sim 2$ Mpc and then approaches a plateau at larger separations. This behaviour suggests that the influence of cluster-scale environments on the intrinsic mass-colour relation is strongest within a few megaparsecs of nodes, beyond which the coupling stabilises. The mass-segregated trends (right panel) clarify the origin of this behaviour. High-mass galaxies exhibit only a weak dependence of I_N on d_n , remaining nearly uniform across the explored range, indicating that their mass-colour connection is relatively insensitive to nodal proximity. In contrast, low-mass galaxies show a pronounced rise in I_N with increasing d_n , extending to $d_n \sim 4$ Mpc before flattening. This stronger and more extended environmental dependence highlights the greater susceptibility of low-mass systems to dynamical processing near nodes, and indicates that the decoupling of mass structure and colour is primarily driven by cluster-scale effects acting on shallow potential wells.

Taken together, Figure 6- Figure 8 demonstrate that the environmental dependence of the mass-colour coupling is intrinsically mass dependent. Nodal environments preferentially disrupt the structural imprint of baryonic composition on colour in low-mass galaxies, while massive systems evolve in a manner more strongly regulated by internal processes. Filaments, on the other hand, preserve and enhance the intrinsic mass-colour linkage by modulating gas supply in a gradual and mass-dependent fashion. The combined behaviour highlights the interplay between internal binding energy and large-scale tidal geometry in shaping the information content shared between galaxy mass structure and evolutionary state.

Figure 9 encapsulates the central physical picture emerging from our analysis: nodes and filaments regulate galaxy evolution through fundamentally different quenching channels. In cluster-scale nodes (left panel), galaxies enter virialised regions characterised by strong tidal fields, hot intracluster media, and enhanced merger rates. These processes drive rapid or externally induced quenching via ram-pressure stripping, tidal heating, and dynamical interactions, often disrupting the intrinsic link between a galaxy's internal mass structure and its star formation activity. In contrast, filament environments (right panel) are governed

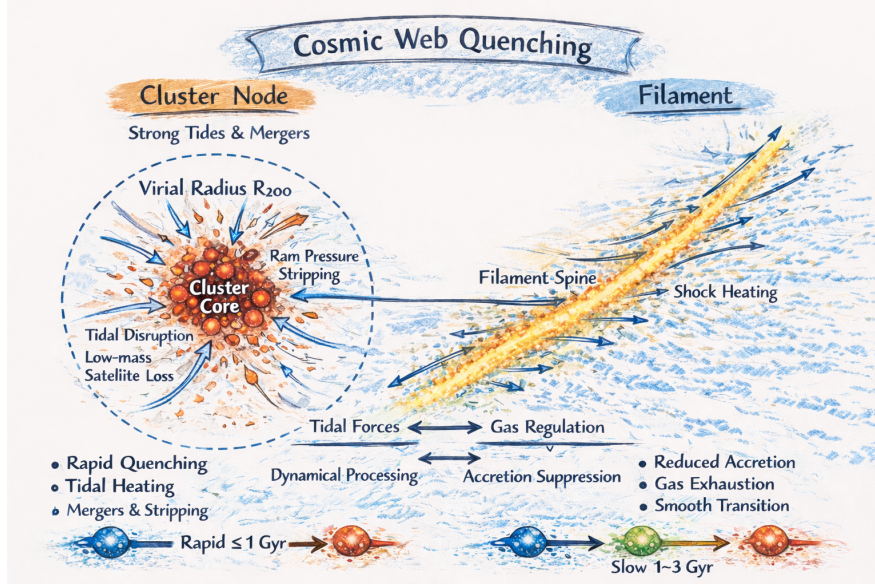


Figure 9. This schematic illustration shows quenching mechanisms in nodes and filaments. Galaxies in cluster environment experience strong tidal fields, ram-pressure stripping, and enhanced merger activity within the virial region ($\sim R_{200}$), leading to rapid or externally driven quenching and partial decoupling between internal mass structure and colour. In filaments, gas and galaxies flow along the filament spine toward nodes. Quenching proceeds gradually through suppression of gas accretion (cosmic web starvation), preserving a stronger coupling between mass composition and colour.

by anisotropic inflows along the spine, where gas and galaxies stream coherently toward nodes. Here quenching proceeds more gradually through the suppression or modulation of cold gas accretion, a form of cosmic web starvation, allowing the colour transformation to remain more tightly coupled to the galaxy’s internal baryonic composition. This highlights the scale-dependent and mechanism-dependent nature of cosmic web quenching: nodes act as nonlinear dynamical processors, whereas filaments function as extended regulators of gas supply.

4 Conclusions

In this work, we have investigated how the two principal structural components of the cosmic web i.e nodes and filaments jointly and independently regulate galaxy evolution. By combining relative colour fractions with an information-theoretic analysis of the coupling between galaxy colour and mass composition, we have uncovered a coherent, scale-dependent picture of cosmic web quenching.

Our analysis of relative red, green, and blue fractions demonstrates that both filament proximity (d_f) and node proximity (d_n) imprint systematic and measurable gradients on galaxy populations. Red galaxies preferentially inhabit regions close to filament spines and nodes, while blue galaxies dominate at larger distances. The characteristic crossover scales ~ 0.75 Mpc for filaments and ~ 2.5 Mpc for nodes are physically meaningful. The node crossover scale is comparable to typical virial radii (R_{200}) of group- and cluster-scale haloes, indicating that quenching becomes efficient once galaxies enter dynamically bound regions. Within $\sim R_{200}$, environmental processes such as ram-pressure stripping, tidal heating, and mergers

operate on timescales comparable to or shorter than the dynamical time ($t_{\text{dyn}} \leq 1 \text{ Gyr}$), driving accelerated transformation toward the red sequence. In contrast, the filament crossover scale traces the transverse extent of dynamically influential filament cores. Here quenching is more gradual and likely regulated by the suppression or modulation of cold gas accretion. Gas depletion over $\sim 1\text{-}3 \text{ Gyr}$ timescales naturally produces a smooth migration from the blue cloud through the green valley to the red sequence. The monotonic dependence of red fraction on d_f and the absence of a sharp turnover indicate that filaments act as extended regulators of gas supply rather than sites of impulsive stripping.

The normalised mutual information analysis provides a complementary and deeper perspective. We find that the statistical coupling between dominant mass component and galaxy colour strengthens with increasing node distance at fixed filament proximity. Near nodes, intense dynamical processing partially erases the intrinsic link between baryonic composition and star formation activity, reducing the predictive power of internal mass structure. Far from nodes, within filament-dominated regions, colour remains more tightly coupled to mass composition, implying that filament-driven quenching is structurally mediated. The mass dependence of this behaviour is particularly revealing. Low-mass galaxies exhibit strong environmental modulation in both relative fractions and mutual information, consistent with their vulnerability to external tidal forces and gas stripping within $\sim R_{200}$. Massive galaxies, by contrast, display flatter environmental trends, indicating that deeper gravitational potentials and internal feedback processes buffer them against environmental decoupling. This dichotomy highlights the interplay between gravitational binding energy and large-scale tidal geometry in shaping galaxy evolution.

These results naturally align with the framework of anisotropic assembly bias. Filaments correspond to regions of one-dimensional collapse, where coherent matter inflow modulates halo growth and gas accretion histories at fixed mass. Nodes represent sites of multi-axial collapse and nonlinear dynamical evolution, where mergers and tidal heating accelerate structural transformation. The observed environmental gradients and the spatial variation of mass-colour coupling together suggest that galaxy properties retain memory of their anisotropic assembly pathways, but that this memory can be partially erased within virialised cluster environments. Cosmic web quenching therefore emerges as a hierarchical and scale-dependent phenomenon. Filaments regulate galaxies over megaparsec scales by modulating gas accretion along coherent tidal directions, while nodes impose rapid dynamical processing within virial radii over dynamical timescales. The combined action of these environments shapes not only the demographic distribution of red and blue galaxies, but also the information content linking internal mass structure to evolutionary state.

In summary, our results demonstrate that galaxy quenching cannot be understood solely in terms of local density or halo mass. The geometry of the cosmic web, encoded through distances to filament spines and nodes plays a fundamental and physically distinct role. By explicitly separating these geometric effects and quantifying their impact through both population statistics and information theory, we provide a unified and physically grounded picture of how large-scale structure sculpts galaxy evolution across cosmic time.

Our results are broadly consistent with earlier studies that reported enhanced red fractions and suppressed star formation in proximity to filaments and nodes, even after controlling for local density. The systematic increase of passive galaxies toward filament spines and cluster-scale nodes reinforces the emerging view that cosmic web geometry encodes environmental information beyond simple overdensity. At the same time, our analysis advances this picture in two important ways. First, by jointly analysing distances to both nodes and

filaments, we disentangle their distinct physical roles, demonstrating that virial-scale dynamical processing in nodes and anisotropic gas regulation in filaments possibly operate through fundamentally different mechanisms. Second, by employing an information-theoretic framework, we show that nodal environments partially erase the intrinsic coupling between mass composition and colour, whereas filamentary environments preserve and even enhance it. This reveals not merely where quenching occurs, but how the underlying structural memory of galaxy assembly is modulated across the cosmic web. Together, these results refine and deepen the geometric paradigm of environmental quenching, providing a more physically resolved understanding of how large-scale structure shapes galaxy evolution.

Looking forward, these results offer several promising avenues for both theoretical refinement and observational validation. On the theoretical side, extending this analysis across redshift would allow direct examination of how virial-scale processing and filamentary regulation evolve with cosmic time, particularly during the peak epoch of star formation when gas accretion rates were higher and cluster environments less dynamically mature. Incorporating halo accretion histories and tidal tensor eigenvalue analyses would further clarify the connection between anisotropic assembly and baryonic transformation. Observationally, forthcoming wide-field spectroscopic surveys such as Euclid [53], DESI [54], and LSST [55] will enable precise reconstruction of the three-dimensional cosmic web over large volumes, allowing measurements of colour fractions and gas content gradients relative to filament spines and cluster nodes. Combining such surveys with HI and molecular gas observations will be particularly powerful in testing the predicted distinction between rapid, virial-scale quenching in nodes and gradual, accretion-regulated quenching in filaments. Ultimately, bridging simulations and observations in this geometrically explicit framework will provide a decisive test of whether anisotropic assembly and cosmic web geometry constitute a fundamental driver of galaxy evolution.

5 Acknowledgements

BP gratefully acknowledges financial support from the Government of India under the project ANRF/ARG/2025/000535/PS. BP also thanks IUCAA, Pune for support received through the Associateship Programme. AD acknowledges Harish-Chandra Research Institute, Allahabad for support provided through a postdoctoral fellowship. The authors extend their gratitude to the Virgo Consortium for providing public access to their simulation data. The EAGLE simulations were performed using the DiRAC-2 facility at Durham, managed by the ICC, and the PRACE facility Curie based in France at TGCC, CEA, Bruyères-le-Châtel.

6 Data availability

The data from the EAGLE simulations employed in this work are publicly available through the EAGLE database (<https://icc.dur.ac.uk/Eagle/database.php>). Any supplementary data products produced in this study are available from the authors upon reasonable request.

References

- [1] S.A. Gregory and L.A. Thompson, *The Coma/A1367 supercluster and its environs.*, *ApJ* **222** (1978) 784.

- [2] M. Joeveer and J. Einasto, *Has the Universe the Cell Structure?*, in *Large Scale Structures in the Universe*, M.S. Longair and J. Einasto, eds., vol. 79 of *IAU Symposium*, p. 241, Jan., 1978.
- [3] J. Einasto, M. Joeveer and E. Saar, *Structure of superclusters and supercluster formation*, *MNRAS* **193** (1980) 353.
- [4] I.B. Zeldovich, J. Einasto and S.F. Shandarin, *Giant voids in the Universe*, *Nature* **300** (1982) 407.
- [5] J. Einasto, A.A. Klypin, E. Saar and S.F. Shandarin, *Structure of superclusters and supercluster formation - III. Quantitative study of the Local Supercluster.*, *MNRAS* **206** (1984) 529.
- [6] J.R. Bond, L. Kofman and D. Pogosyan, *How filaments of galaxies are woven into the cosmic web*, *Nature* **380** (1996) 603 [[astro-ph/9512141](#)].
- [7] S. Bharadwaj, V. Sahni, B.S. Sathyaprakash, S.F. Shandarin and C. Yess, *Evidence for Filamentarity in the Las Campanas Redshift Survey*, *ApJ* **528** (2000) 21 [[astro-ph/9904406](#)].
- [8] B. Pandey and S. Bharadwaj, *A two-dimensional analysis of percolation and filamentarity in the Sloan Digital Sky Survey Data Release One*, *MNRAS* **357** (2005) 1068 [[astro-ph/0409616](#)].
- [9] M.A. Aragón-Calvo, R. van de Weygaert and B.J.T. Jones, *Multiscale phenomenology of the cosmic web*, *MNRAS* **408** (2010) 2163 [[1007.0742](#)].
- [10] M. Cautun, R. van de Weygaert, B.J.T. Jones and C.S. Frenk, *Evolution of the cosmic web*, *MNRAS* **441** (2014) 2923 [[1401.7866](#)].
- [11] N.I. Libeskind, R. van de Weygaert, M. Cautun, B. Falck, E. Tempel, T. Abel et al., *Tracing the cosmic web*, *MNRAS* **473** (2018) 1195 [[1705.03021](#)].
- [12] B. Pandey and S. Bharadwaj, *The luminosity, colour and morphology dependence of galaxy filaments in the Sloan Digital Sky Survey Data Release Four*, *MNRAS* **372** (2006) 827 [[astro-ph/0601179](#)].
- [13] B. Pandey and S. Bharadwaj, *Exploring star formation using the filaments in the Sloan Digital Sky Survey Data Release Five*, *MNRAS* **387** (2008) 767 [[0804.0072](#)].
- [14] S.C. Porter and S. Raychaudhury, *Star formation in galaxies along the Pisces-Cetus Supercluster filaments*, *MNRAS* **375** (2007) 1409 [[astro-ph/0612357](#)].
- [15] S.C. Porter, S. Raychaudhury, K.A. Pimblet and M.J. Drinkwater, *Star formation in galaxies falling into clusters along supercluster-scale filaments*, *MNRAS* **388** (2008) 1152 [[0804.4177](#)].
- [16] T. Kuutma, A. Tamm and E. Tempel, *From voids to filaments: environmental transformations of galaxies in the SDSS*, *A&A* **600** (2017) L6 [[1703.04338](#)].
- [17] N. Malavasi, S. Arnouts, D. Vibert, S. de la Torre, T. Moutard, C. Pichon et al., *The VIMOS Public Extragalactic Redshift Survey (VIPERS): galaxy segregation inside filaments at $z \approx 0.7$* , *MNRAS* **465** (2017) 3817 [[1611.07045](#)].
- [18] C. Laigle, C. Pichon, S. Arnouts, H.J. McCracken, Y. Dubois, J. Devriendt et al., *COSMOS2015 photometric redshifts probe the impact of filaments on galaxy properties*, *MNRAS* **474** (2018) 5437 [[1702.08810](#)].
- [19] K. Kraljic, S. Arnouts, C. Pichon, C. Laigle, S. de la Torre, D. Vibert et al., *Galaxy evolution in the metric of the cosmic web*, *MNRAS* **474** (2018) 547.
- [20] V. Bonjean, N. Aghanim, M. Douspis, N. Malavasi and H. Tanimura, *Sunyaev-zel'dovich and lensing signatures of gas in cosmic filaments*, *A&A* **638** (2020) A75.
- [21] B. Pandey and S. Sarkar, *Exploring galaxy colour in different environments of the cosmic web with SDSS*, *MNRAS* **498** (2020) 6069 [[2002.08400](#)].
- [22] T.-E. Bulichi, R. Davé and K. Kraljic, *How galaxy properties vary with filament proximity in the SIMBA simulations*, *MNRAS* **529** (2024) 2595 [[2309.03282](#)].

- [23] I. Strateva, Ž. Ivezić, G.R. Knapp, V.K. Narayanan, M.A. Strauss, J.E. Gunn et al., *Color Separation of Galaxy Types in the Sloan Digital Sky Survey Imaging Data*, *AJ* **122** (2001) 1861 [[astro-ph/0107201](#)].
- [24] M.R. Blanton, D.W. Hogg, N.A. Bahcall, I.K. Baldry, J. Brinkmann, I. Csabai et al., *The Broadband Optical Properties of Galaxies with Redshifts $0.02 < z < 0.22$* , *ApJ* **594** (2003) 186 [[astro-ph/0209479](#)].
- [25] E.F. Bell, D.H. McIntosh, N. Katz and M.D. Weinberg, *The Optical and Near-Infrared Properties of Galaxies. I. Luminosity and Stellar Mass Functions*, *ApJS* **149** (2003) 289 [[astro-ph/0302543](#)].
- [26] M.L. Balogh, I.K. Baldry, R. Nichol, C. Miller, R. Bower and K. Glazebrook, *The Bimodal Galaxy Color Distribution: Dependence on Luminosity and Environment*, *ApJ Letters* **615** (2004) L101 [[astro-ph/0406266](#)].
- [27] I.K. Baldry, K. Glazebrook, J. Brinkmann, Ž. Ivezić, R.H. Lupton, R.C. Nichol et al., *Quantifying the Bimodal Color-Magnitude Distribution of Galaxies*, *ApJ* **600** (2004) 681 [[astro-ph/0309710](#)].
- [28] T.K. Wyder, D.C. Martin, D. Schiminovich, M. Seibert, T. Budavári, M.A. Treyer et al., *The UV-Optical Galaxy Color-Magnitude Diagram. I. Basic Properties*, *ApJS* **173** (2007) 293 [[0706.3938](#)].
- [29] S. Salim, *Green Valley Galaxies*, *Serbian Astronomical Journal* **189** (2014) 1 [[1501.01963](#)].
- [30] K. Schawinski, C.M. Urry, B.D. Simmons, L. Fortson, S. Kaviraj, W.C. Keel et al., *The green valley is a red herring: Galaxy Zoo reveals two evolutionary pathways towards quenching of star formation in early- and late-type galaxies*, *MNRAS* **440** (2014) 889 [[1402.4814](#)].
- [31] A. Das, B. Pandey and S. Sarkar, *Green valley galaxies in the cosmic web: internal versus environmental quenching*, *JCAP* **2021** (2021) 045 [[2101.02564](#)].
- [32] A. Das and B. Pandey, *The long road to the Green Valley: Tracing the evolution of the Green Valley galaxies in the EAGLE simulation*, *JCAP* **2025** (2025) 101 [[2501.01207](#)].
- [33] M. Hoosain, S.L. Blyth, R.E. Skelton and et al., *The effect of cosmic web filaments on galaxy properties in the resolve and manga samples*, *MNRAS* **528** (2024) 4139.
- [34] S. Zarattini and J.A.L. Aguerri, *Galaxy transformation across the cosmic web: Evolution of stellar colours and star formation rates in filaments*, *A&A* **698** (2025) A196 [[2504.02026](#)].
- [35] A. Nandi, B. Pandey and P. Sarkar, *The correlations between galaxy properties in different environments of the cosmic web*, *JCAP* **2024** (2024) 012 [[2306.05354](#)].
- [36] A. Nandi and B. Pandey, *Impact of cosmic web on galaxy properties and their correlations: Insights from Principal Component Analysis*, *Astronomy and Computing* **53** (2025) 100972 [[2408.16731](#)].
- [37] A. Nandi, B. Pandey and P. Sarkar, *Tracing correlations between galaxy properties across the Cosmic Web: An IllustrisTNG-based study*, *Astronomy and Computing* **55** (2026) 101023 [[2509.11288](#)].
- [38] A. Nandi and B. Pandey, *Galaxy quenching across the Cosmic Web: disentangling mass and environment with SDSS DR18*, *arXiv e-prints* (2025) arXiv:2507.18614 [[2507.18614](#)].
- [39] B. Pandey, *Tracing the green valley with entropic thresholding*, *MNRAS* **530** (2024) 4550 [[2306.09395](#)].
- [40] J. Schaye, R.A. Crain, R.G. Bower, M. Furlong, M. Schaller, T. Theuns et al., *The EAGLE project: simulating the evolution and assembly of galaxies and their environments*, *MNRAS* **446** (2015) 521 [[1407.7040](#)].

- [41] R.A. Crain, J. Schaye, R.G. Bower, M. Furlong, M. Schaller, T. Theuns et al., *The EAGLE simulations of galaxy formation: calibration of subgrid physics and model variations*, *MNRAS* **450** (2015) 1937 [[1501.01311](#)].
- [42] PLANCK collaboration, *Planck 2013 results. I. Overview of products and scientific results*, *Astron. Astrophys.* **571** (2014) A1 [[1303.5062](#)].
- [43] V. Springel, S.D.M. White, A. Jenkins, C.S. Frenk et al., *Simulations of the formation, evolution and clustering of galaxies and quasars*, *Nature* **435** (2005) 629.
- [44] V. Springel, S.D.M. White, G. Tormen and G. Kauffmann, *Populating a cluster of galaxies - I. Results at $z=0$* , *MNRAS* **328** (2001) 726 [[astro-ph/0012055](#)].
- [45] S. McAlpine, J.C. Helly, M. Schaller, J.W. Trayford, Y. Qu, M. Furlong et al., *The EAGLE simulations of galaxy formation: Public release of halo and galaxy catalogues*, *Astronomy and Computing* **15** (2016) 72 [[1510.01320](#)].
- [46] B. Pandey, *Separating the blue cloud and the red sequence using Otsu’s method for image segmentation*, *Astronomy and Computing* **44** (2023) 100725 [[2211.15642](#)].
- [47] J.N. Kapur, P.K. Sahoo and A.K.C. Wong, *A new method for gray-level picture thresholding using the entropy of the histogram*, *Computer Vision, Graphics, and Image Processing* **29** (1985) 273.
- [48] T. Sousbie, C. Pichon and H. Kawahara, *The persistent cosmic web and its filamentary structure - II. Illustrations*, *MNRAS* **414** (2011) 384 [[1009.4014](#)].
- [49] T. Sousbie, *The persistent cosmic web and its filamentary structure - I. Theory and implementation*, *MNRAS* **414** (2011) 350 [[1009.4015](#)].
- [50] W.E. Schaap and R. van de Weygaert, *Continuous fields and discrete samples: reconstruction through Delaunay tessellations*, *A&A* **363** (2000) L29 [[astro-ph/0011007](#)].
- [51] R. van de Weygaert and W. Schaap, *The Cosmic Web: Geometric Analysis*, in *Data Analysis in Cosmology*, V.J. Martínez, E. Saar, E. Martínez-González and M.J. Pons-Bordería, eds., vol. 665, pp. 291–413 (2009), [DOI](#).
- [52] C.E. Shannon, *A mathematical theory of communication*, *The Bell System Technical Journal* **27** (1948) 379.
- [53] Euclid Collaboration, Y. Mellier, Abdurro’uf, J.A. Acevedo Barroso, A. Achúcarro, J. Adamek et al., *Euclid: I. Overview of the Euclid mission*, *A&A* **697** (2025) A1 [[2405.13491](#)].
- [54] DESI Collaboration, M. Abdul-Karim, A.G. Adame, D. Aguado, J. Aguilar, S. Ahlen et al., *Data Release 1 of the Dark Energy Spectroscopic Instrument*, *arXiv e-prints* (2025) [arXiv:2503.14745](#) [[2503.14745](#)].
- [55] Ž. Ivezić, S.M. Kahn, J.A. Tyson, B. Abel, E. Acosta, R. Allsman et al., *LSSST: From Science Drivers to Reference Design and Anticipated Data Products*, *ApJ* **873** (2019) 111 [[0805.2366](#)].